CrossMark
click for updates

Investigation of the Lipid Binding Properties of the Marburg Virus Matrix Protein VP40

Kaveesha J. Wijesinghe,[a] Robert V. Stahelin[a,b]

Department of Chemistry and Biochemistry, Eck Institute for Global Health, and Boler-Parseghian Center for Rare and Neglected Diseases, University of Notre Dame, Notre Dame, Indiana, USA[a]; Department of Biochemistry and Molecular Biology, Indiana University School of Medicine—South Bend, South Bend, Indiana, USA[b]

ABSTRACT
Marburg virus (MARV), which belongs to the virus family *Filoviridae*, causes hemorrhagic fever in humans and nonhuman primates that is often fatal. MARV is a lipid-enveloped virus that during the replication process extracts its lipid coat from the plasma membrane of the host cell it infects. MARV carries seven genes, one of which encodes its matrix protein VP40 (mVP40), which regulates the assembly and budding of the virions. Currently, little information is available on mVP40 lipid binding properties. Here, we have investigated the *in vitro* and cellular mechanisms by which mVP40 associates with lipid membranes. mVP40 associates with anionic membranes in a nonspecific manner that is dependent upon the anionic charge density of the membrane. These results are consistent with recent structural determination of mVP40, which elucidated an mVP40 dimer with a flat and extensive cationic lipid binding interface.

IMPORTANCE
Marburg virus (MARV) is a lipid-enveloped filamentous virus from the family *Filoviridae*. MARV was discovered in 1967, and yet little is known about how its seven genes are used to assemble and form a new viral particle in the host cell it infects. The MARV matrix protein VP40 (mVP40) underlies the inner leaflet of the virus and regulates budding from the host cell plasma membrane. *In vitro* and cellular assays in this study investigated the mechanism by which mVP40 associates with lipids. The results demonstrate that mVP40 interactions with lipid vesicles or the inner leaflet of the plasma membrane are electrostatic but nonspecific in nature and are dependent on the anionic charge density of the membrane surface. Small molecules that can disrupt lipid trafficking or reduce the anionic charge of the plasma membrane interface may be useful in inhibiting assembly and budding of MARV.

Marburg virus (MARV) and Ebola virus (EBOV) are members of the virus family *Filoviridae* that are characterized by their filamentous lipid-enveloped morphology (1). Electron microscopy studies revealed that MARV particles have a uniform diameter of approximately 80 nm, with an average particle length of 740 nm (2, 3). MARV harbors a negative-sense RNA genome 19.1 kb in length that includes seven genes (4). The glycoprotein (GP) is a transmembrane protein present in the viral envelope, and it mediates viral entry into the host cell. VP40 is the major matrix protein (mVP40) and completely underlies the lipid envelope of the virus. VP40 alone is sufficient to produce virus-like particles (VLPs) from mammalian cells that are nearly indistinguishable from virions (5–8). In addition to interacting with the host cell membrane and mediating budding, VP40 interacts with the nucleocapsid, which consists of nucleoprotein, VP24, VP30, VP35, and the L protein (9). VP40 also plays other essential roles, such as immunosuppression (10), regulation of viral transcription, and/or replication (11, 12), and is also able to interact with GP, coexpression of which leads to GP enrichment at sites of mVP40 budding (13).

mVP40 is a peripheral protein that is trafficked to the plasma membrane along the retrograde late endosomal pathway (14). This trafficking mechanism is likely different than that of the EBOV VP40 matrix protein (eVP40), which has been shown to be transported in a COPII vesicle-dependent manner (15). mVP40 and eVP40 are 34% identical (49% homologous) in amino acid sequence, which suggests they may have some different interactions with host cell proteins or lipids. eVP40 harbors an N-terminal domain (NTD) involved in oligomerization (16–19) and a C-terminal domain (CTD) reported to mediate membrane binding (20–25). Recent structural analyses of eVP40 (21) and mVP40 (26) have revealed an NTD interface that mediates dimerization, which is required for VP40 plasma membrane localization and budding. The NTDs have 42% sequence identity and similar folds, while the CTD is only 15% identical in sequence and somewhat different in structure (26). This suggests that eVP40 and mVP40 may have different membrane binding properties mediated by CTD interactions with the plasma membrane interface.

The inner leaflet of the plasma membrane is enriched in anionic phospholipids, including phosphatidylserine (PS) (27), phosphatidylinositol-4-phosphate [PI(4)P] (28), and phosphatidylinositol-4,5-bisphosphate [PI(4,5)P_2] (29). These anionic phospholipids, which comprise about 20 to 30 mol% of the plasma membrane inner leaflet, provide platforms for peripheral proteins to mediate membrane association by using exposed basic residues on the surface of the protein (30, 31). PS is the most

abundant anionic phospholipid found at the inner leaflet of the membrane, containing up to 15 to 20 mol% (32), and provides points of attachment for peripheral proteins that contain specific PS binding domains, such as C2 domains (33), or association with proteins containing polybasic clusters through nonspecific electrostatic interactions (34). Similarly, proteins that interact with plasma membrane $PI(4,5)P_2$ may do so with a specific binding motif (35–37) or through nonspecific electrostatic interactions (30, 31). Not surprisingly, several viral matrix proteins, including eVP40 (20, 22–25, 38), have been shown to associate with anionic lipids, such as PS and $PI(4,5)P_2$, *in vitro* and in cells (39–46), which is important in mediating their assembly and budding.

In this study, we employed *in vitro* lipid binding assays and cellular localization analysis to investigate mVP40 lipid binding properties. The results indicate that mVP40 interacts with anionic phospholipids in a nonspecific manner, functioning as an anionic charge sensor. mVP40 binding to membranes is dependent upon the anionic charge density of the plasma membrane, which when neutralized ablates mVP40 localization. The binding and cellular localization of mVP40 are consistent with recent structural analysis demonstrating that mVP40 has a flat and extensive CTD basic surface (26).

MATERIALS AND METHODS

Materials. All lipids were purchased from Avanti Polar Lipids (Alabaster, AL) and used without further purification. Complete Mini-EDTA-free protease inhibitor cocktail was from Roche (Indianapolis, IN), and phenylmethylsulfonylfluoride (PMSF) and bicinchoninic acid (BCA) protein assay kits were from Thermo Fisher Scientific (Waltham, MA). Lipofectamine 2000 and Lipofectamine LTX were from Life Technologies (Grand Island, NY). Ni-nitrilotriacetic acid (NTA) agarose was from Qiagen (Valencia, CA).

mVP40-His tag in pET46 was a kind gift from E. Ollmann Saphire (The Scripps Research Institute). The KR-ϕ–mRFP and GFP–R-Pre plasmids were a kind gift from Sergio Grinstein (University of Toronto), and PLCδ-PH green fluorescent protein (GFP) was a kind gift from Tamas Balla (NIH). Myc-5–phosphatase wild type (WT) and a Myc-5–phosphatase catalytically inactive deletion mutant were kind gifts from P. Majerus (Washington University) (44, 47). Monomeric red fluorescent protein (mRFP)-FKBP-pseudojanin (PJ-WT), mRFP-FKBP-Sac1, mRFP-FKBP-INPP5E, and Lyn11-FRB-CFP (cyan fluorescent protein) were kind gifts from Tamas Balla (NIH) and Gerald Hammond (University of Pittsburgh).

Protein purification. In order express and purify mVP40, the mVP40-His tag pET46 plasmid was transformed into *Escherichia coli* Rosetta (pLysS) cells. Successfully transformed pLysS cell colonies were used to inoculate 3 ml of LB medium containing 100 μg/ml ampicillin. This 3-ml preculture was grown overnight at 37°C with shaking (200 rpm) and was used to inoculate 1 liter LB medium containing 100 μg/ml ampicillin. Cells were grown with shaking (200 rpm) at 37°C until the optical density at 600 nm reached 0.6. Expression of mVP40 protein was induced at 25°C by treating the cells with 0.1 mM IPTG (isopropyl-β-D-thiogalactopyranoside) for 5 h or with 0.025 mM IPTG overnight. The cells were then harvested by centrifugation at 6,000 × g for 10 min. The cells were resuspended in lysis buffer (50 mM NaH_2PO_4, 300 mM NaCl, 10 mM imidazole, pH 8.0) and incubated for 15 min after adding 100 mM phenylmethylsulfonyl fluoride (PMSF) to a final concentration of 0.1 mM, lysozyme to a final concentration of 1 mg/ml, and 10 μl of 100× protease inhibitor for each 10 ml of lysate buffer.

Following incubation, the lysate was sonicated at 4°C using multiple short pulses (10 s) with pauses (30 s). The lysate was then centrifuged at 50,000 × g for 20 min, and the supernatant was filtered sequentially through 0.8-μm and 0.45-μm filters. The filtered supernatant was incu-

bated with Ni-NTA agarose resin for 1 h at 4°C with gentle shaking. Lysate with the Ni-NTA resin was applied to a column, and the flowthrough was discarded. The column was washed with 15 ml of wash buffer (50 mM NaH_2PO_4, pH 8.0, containing 300 mM NaCl and 30 mM imidazole, pH 8.0), and the mVP40 protein was eluted with 7 ml of elution buffer (50 mM NaH_2PO_4, pH 8.0, containing 300 mM NaCl and 250 mM imidazole). The eluted protein was dialyzed overnight at 4°C with gentle stirring against 25 mM HEPES, pH 7.4, containing 150 mM KCl. After dialysis, mVP40 proteins were concentrated using a 10,000-Da Amicon ultracentrifugation filter (Merck Millipore Ltd., Billerica, MA) by centrifuging at 4,000 × g.

MLV sedimentation assay. 1-Palmitoyl-2-oleoyl-*sn*-glycero-3-phosphocholine (POPC), 1-palmitoyl-2-oleoyl-*sn*-glycero-3-phosphoethanolamine (POPE), 1-palmitoyl-2-oleoyl-*sn*-glycero-3-phospho-L-serine (POPS), phosphatidylinositol derivatives (PIPs), and 1,2-dioleoyl-*sn*-glycero-3-phosphate (PA) were mixed in the indicated molar ratios and dried under N_2 gas for 10 min. In all sedimentation assays, 30% POPE, 20% POPS, and 5% PIPs were used to maintain consistency (unless otherwise stated), and POPC levels were scaled accordingly. Lipids were hydrated with resuspension buffer (25 mM HEPES, pH 7.4, containing 150 mM KCl) and incubated at 37°C for 15 min to facilitate hydration of lipids to form vigorously vortexed multilamellar vesicles (MLVs) (48–52). These lipid solutions were then incubated with 5 μM mVP40 proteins at room temperature for 20 min. The total assay volume was 100 μl, and the final lipid concentration was 1 mM. Samples were centrifuged at 48,000 × g for 20 min. During centrifugation, MARV VP40 bound with MLVs sedimented, while unbound proteins remained in the supernatant. The supernatant was carefully removed from the pellet, and the pellet was resuspended in an amount of buffer equal to the volume that was removed as the supernatant. Forty microliters from each supernatant and pellet sample was separated by SDS-PAGE, and following staining with Coomassie brilliant blue, gel band intensities were analyzed in the gel images using Image J software. For quantification, the gel images were first converted to 8-bit images using Image J software. Using the rectangular selection tool, a rectangular region around the gel bands was selected and marked as the first lane. By selecting plot lanes, the software creates a graphical representation of the band intensities as peaks, and by using the wand tool, the area under the peak for each gel band is obtained. The fraction of proteins associated with MLVs of each lipid composition were calculated by the following ratio: area under the peak for the pellet gel band divided by the area under the peak for supernatant plus pellet gel bands. Each experiment was performed at least three times to calculate a mean, standard deviation (SD) (or standard error of the mean [SEM] when indicated), and *P* value.

Cell culture. COS-7 cells were maintained in Dulbecco's modified Eagle's medium (DMEM) (Invitrogen) containing 10% FBS and 1% Penstrep at 37°C in a 5% CO_2 humidified incubator. The cells were grown to 70 to 80% confluence before passaging or transfection. Transfections were performed using Lipofectamine 2000 reagent according to the manufacturer's protocol.

Pharmacological treatments. Pharmacological treatments were performed at 37°C unless otherwise noted. A sphingosine stock solution was made by evaporation of chloroform under nitrogen gas. The resulting film was then resuspended in ethanol. Sphingosine was then added to cells in culture to a final concentration of 75 μM. Ethanol at the same final percentage as in the delivery experiment was used as the vehicle control.

Confocal imaging and analysis. Routine imaging of all cell lines was performed on a Zeiss LSM 710 inverted microscope using a Plan Apochromat 63× 1.4-numerical-aperture oil objective, and either the 488-nm or 561-nm laser line or both laser lines were used for colocalization/dual-visualization experiments. The laser power was maintained constant during the experiment (at 1.0), as were the gain and offset settings. Enhanced green fluorescent protein (EGFP) was imaged using the 488-nm line of the Ar ion laser, with the emission collected from 493- to 550-nm. mRFP was excited with emission from the 561-nm laser line, and the emission was collected from 600 to 700 nm. Unless otherwise stated, cells were imaged
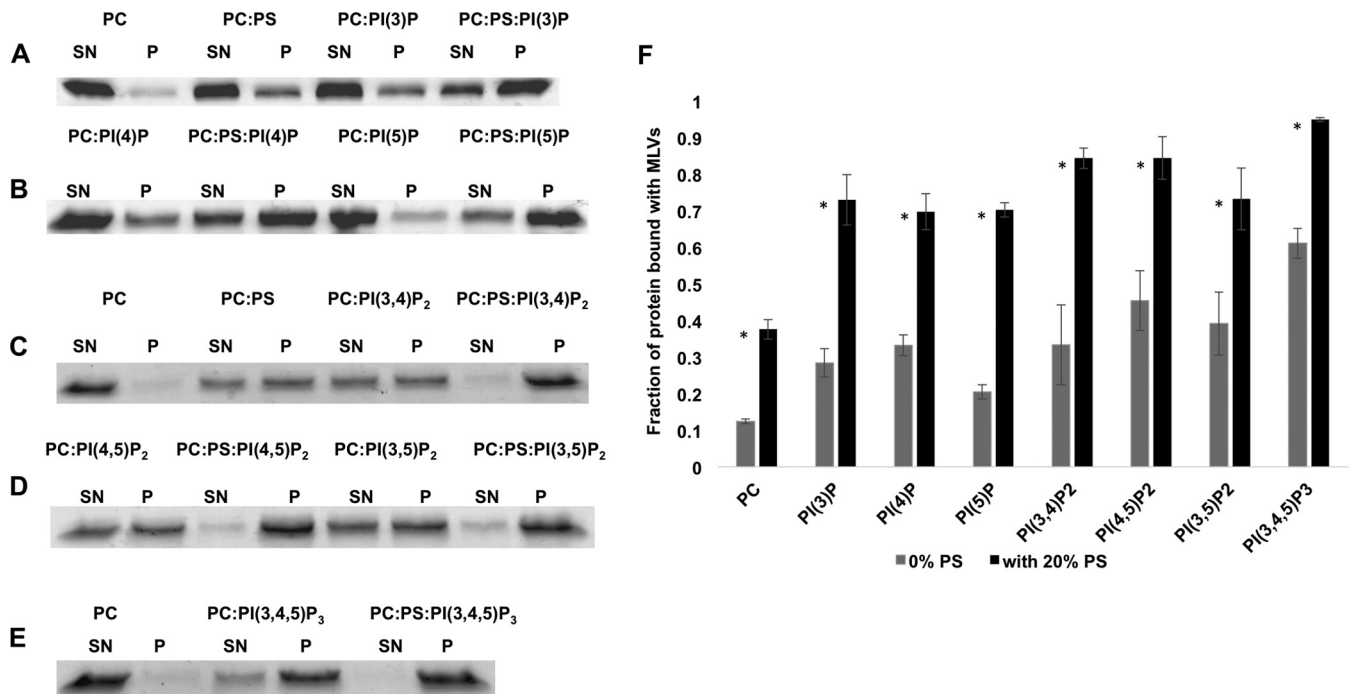
FIG 1 Assessment of mVP40 association with lipid vesicles containing different PIPs or PS. (A to E) SDS-PAGE of supernatant (SN) and pellet (P) fractions collected from MLV sedimentation assays on lipid compositions shown above the gels. In all liposomes, 30 mol% of PE was used, and when shown, 5 mol% phosphoinositide or 20 mol% PS was used to maintain consistency. Thus, control vesicles consisted of 70 mol% POPC and 30% POPE. PS or PIPs were then added to the vesicles at the expense of POPC. (F) Quantification of MLV sedimentation assay results using Image J. The data represent the averages of three sedimentation assays, with the error bars representing the standard errors of the mean. *, $P < 0.05$.

12 h posttransfection. In experiments where cells were imaged for quantification for localization (mVP40, PLCδ-PH GFP, or KR-φ–mRFP), at least 10 cells were imaged and quantified in each experiment, and three replicates of each experiment were performed and averaged to calculate the standard deviation (or standard error of the mean, if indicated), as well as the P value. Image J software was used to assess the plasma membrane and cytoplasmic intensities. Using the free-hand tool on the image J software, regions on the plasma membrane or the cytoplasm in the cell image were selected. Using the analyze tool, the intensity and the area of the selected region were obtained to calculate the intensity per pixel. Likewise, multiple regions on the plasma membrane and the cytoplasm (up to 6 regions) were selected to obtain the average plasma membrane intensity per pixel and average cytoplasmic intensity per pixel, respectively. These averaged values were used to calculate the ratio [plasma membrane intensity/(plasma membrane + cytoplasmic intensity)] for quantification of plasma membrane and cytoplasmic distributions of MARV VP40 and also for assessment of localization.

For the rapamycin-induced phosphoinositide depletion system (28), Cos-7 cells were transfected with Lyn11-FRB-CFP; (PJ-WT, INPP5E, Sac1, or PJ-Dead)-FKBP-mRFP; and either PLCδ-PH-EGFP, R-Pre–GFP, or EGFP-MARV-VP40. Fourteen hours posttransfection, cells were treated with 1 μM (final concentration) rapamycin (Sigma) for 7 min during imaging on a Zeiss LSM 710 as described above. Cell images at time zero and at 7 min were analyzed as described previously to obtain the average intensity per pixel for the plasma membrane and cytoplasm at time zero and 7 min. The dissociation index was calculated for each EGFP construct after depletion with each pseudojanin (PJ) construct as previously described by Hammond et al. (28) using the following equation: dissociation index = (PM intensity/Cyto intensity)$_{before}$/(PM intensity/Cyto intensity)$_{after}$, where PM represents plasma membrane and Cyto represents cytoplasmic. Real-time imaging of 4 different cells was done for each PJ construct to obtain the mean dissociation index and the standard error of the mean.

RESULTS

Assessment of mVP40 binding to lipid vesicles that contained PS and/or PIPs. MLV sedimentation assays are useful tools to understand the membrane binding properties of lipid binding proteins. In these assays, mVP40 was incubated with MLVs of different lipid compositions to assess mVP40 lipid selectivity for different anionic phospholipids. After incubation, the assay mixture was centrifuged to pellet the MLVs. The appearance of mVP40 in the pellet reflected the proteins that were bound to MLVs, while the unbound mVP40 remained in the supernatant.

The results demonstrated that mVP40 bound MLVs composed of anionic phospholipids, such as PS and PIPs (Fig. 1). The data indicated that vesicles containing anionic PS exhibited a 4-fold increase in mVP40 binding compared to those composed solely of zwitterionic phosphocholine (PC) and phosphatidylethanolamine (PE) (Fig. 1A and F). Additionally, mVP40 showed significant binding to MLVs that contained 5 mol% PIPs. mVP40 bound to MLVs containing PI(3)P, PI(4)P, or PI(5)P, with similar fractions of protein bound. These results suggested mVP40 did not significantly differentiate between the positions of the phosphate group on the inositol moiety (Fig. 1A, B, and F). When MLVs containing both 20% PS and 5% PIP were employed, mVP40 association with the membranes was significantly increased, and the effects of both PS and PIP were additive. mVP40 showed similar patterns of binding with MLVs containing 5 mol% phosphatidylinositol bisphosphates [PI(3,4)P$_2$, PI(4,5)P$_2$, or PI(3,5)P$_2$] and phosphatidylinositol trisphosphate [PI(3,4,5)P$_3$] in the presence or absence of PS (Fig. 1C to F). These data suggested that mVP40 lacked specificity for a particular anionic phos-
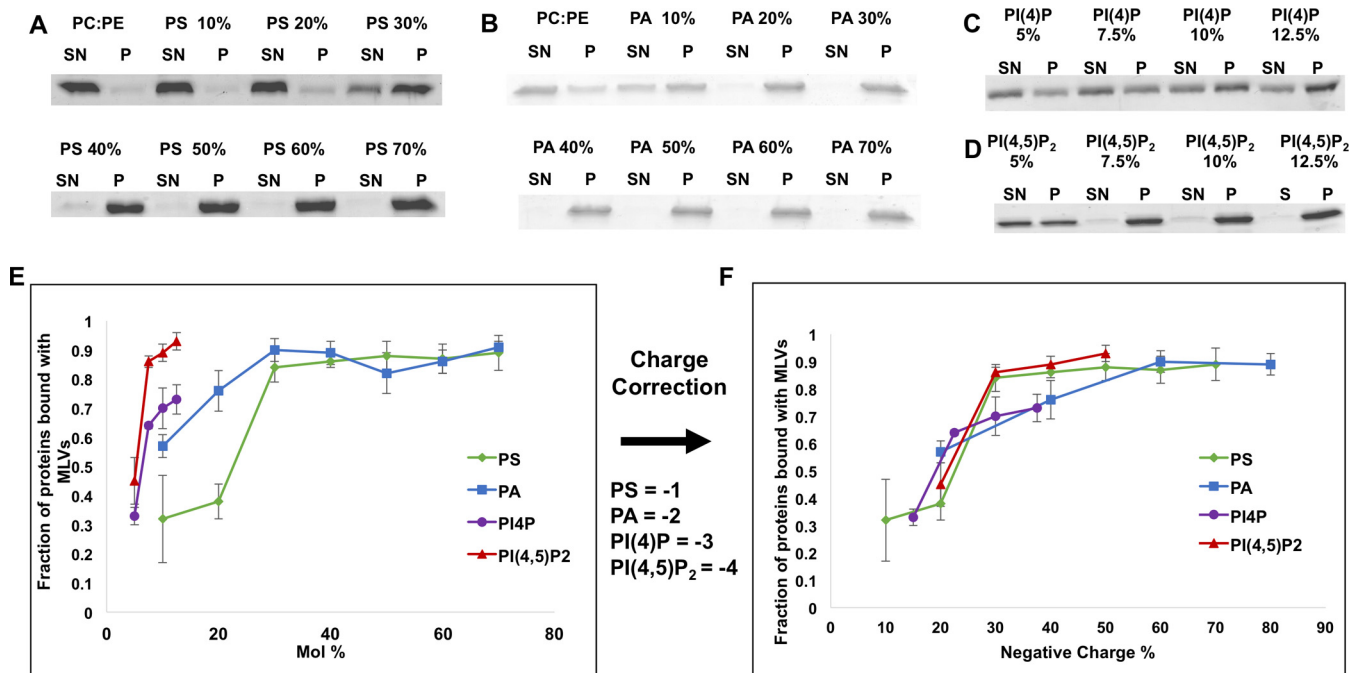
FIG 2 MARV VP40 association with anionic membranes is nonspecific and charge dependent. (A to D) SDS-PAGE of supernatant (SN) and pellet (P) fractions collected from MLV sedimentation assays on lipid compositions shown above the gels. In all liposomes, 30 mol% POPE was used to maintain consistency, and POPC levels were changed accordingly when anionic lipid was added. (E) Quantification of MLV sedimentation assay data for PS, PA, PI(4)P, and PI(4,5)P$_2$ concentration gradients. The data represent the averages of at least three sedimentation assays, with the error bars representing the standard errors of the mean. (F) Fractions of proteins bound to MLVs as a function of the amount of anionic charge present on the vesicles.

pholipid but demonstrated increased association with membranes as the anionic charge density present in the membranes increased.

If mVP40 lipid binding is indeed dependent on the anionic charge density, mVP40 should exhibit increased association with MLVs in response to the concentration gradient of anionic phospholipids. Therefore, we examined mVP40 interactions with MLVs as the concentration of PS was increased from 10 mol% to 70 mol%. As we hypothesized, a gradual increase in mVP40 association with the MLVs was observed as the PS concentration increased, reaching saturation of the binding signal when the PS concentration reached 40 to 50 mol% (Fig. 2A and E). Next, we determined the mVP40 fraction bound with other anionic phospholipid gradients, PA, PI(4)P, and PI(4,5)P$_2$. All of these anionic phospholipids promoted mVP40 association as their concentrations were increased (Fig. 2B to D). mVP40 demonstrated saturation in association with MLVs when the PA concentration reached 30 mol% (Fig. 2B and E) and when the PI(4,5)P$_2$ concentration reached 7.5 mol% (Fig. 2D and E). The difference in the saturation concentrations of these anionic phospholipids reflects the amounts of anionic charges they carry at physiological pH. PS carries a single charge, PI(4)P has approximately 3, and PI(4,5)P$_2$ has approximately 4 anionic charges at pH 7.4 (53). PA in the presence of PE favors the fully deprotonated form and therefore carries two anionic charges (54). Therefore, taking the respective anionic charges present on these different phospholipids into account, we replotted the mVP40 association with the membrane as a function of the percent anionic charge present on the MLVs. After the charge correction, the binding curves nearly overlapped (Fig. 2F). These results confirmed that mVP40 did not discriminate between anionic phospholipid head groups and bound lipid membranes as a function of anionic charge density.

In order to ensure that the 30% POPE was not causing significant phase changes in MLVs, we used laurdan steady-state fluorescence experiments to probe the membrane structures of the MLVs we used for sedimentation assay experiments (55–58). We did observe a slight blue shift in the laurdan assay when POPE was present in the MLVs (data not shown), but this change was not significant, as the general polarization values were indicative of the liquid disordered phase (data not shown). We also used surface plasmon resonance (SPR) measurements to determine if the presence of POPE significantly influenced binding of mVP40 to membranes containing POPS. The apparent K_d (dissociation constant) values for mVP40 with POPC-POPS (80:20) or POPC-POPE-POPS (60:20:20) were very similar (~1,500 nM and ~1,850 nM, respectively, at pH 7.4 and 150 mM KCl) (data not shown). Under similar conditions, the apparent K_d of eVP40 has been reported to be ~300 nM, suggesting eVP40 may have higher apparent affinity for POPS-containing vesicles under similar assay conditions (24, 59).

Plasma membrane localization of MARV VP40 is dependent upon the anionic charge of the cytoplasmic leaflet. Next, we examined the importance of the net anionic charge present on the plasma membrane inner leaflet in live COS-7 cells for mVP40 localization. Sphingosine, which carries a single positive charge, has been shown previously to neutralize the anionic charge of the plasma membrane (27). Delivery of sphingosine induced a significant loss of plasma membrane localization of proteins that interact with the plasma membrane based upon the anionic charge density but not of those proteins that specifically coordinate a lipid
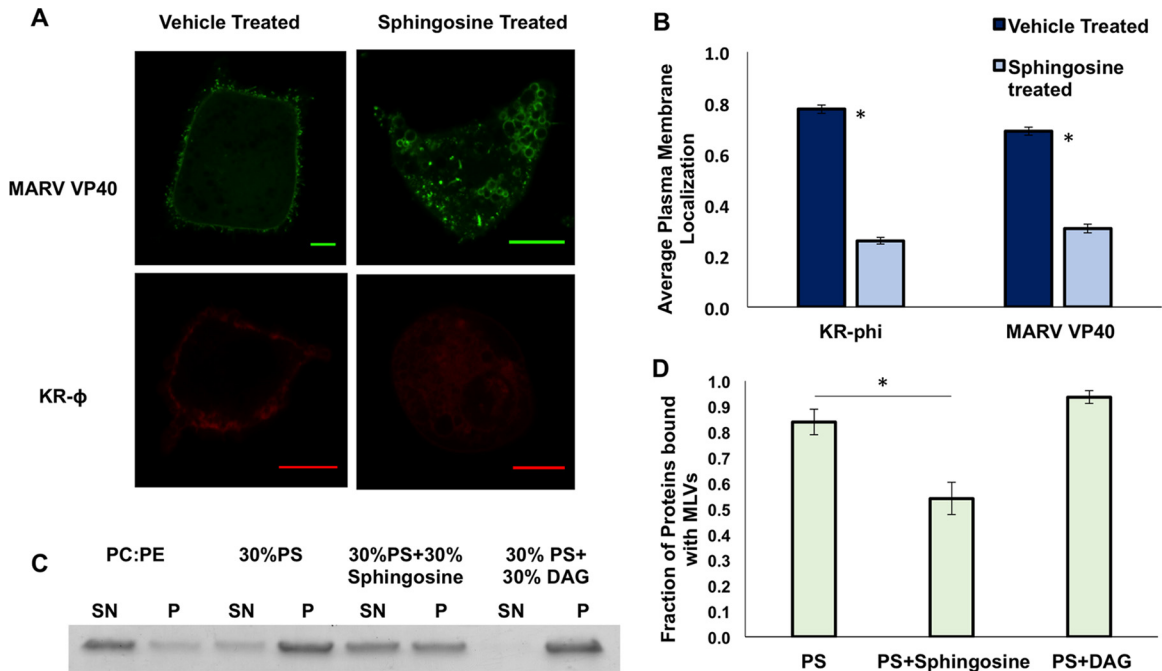
FIG 3 MARV VP40 plasma membrane localization and membrane binding with and without charge neutralization. (A) COS-7 cells expressing fluorescent fusion constructs of EGFP-mVP40 or mRFP–KR-ϕ after 2 h of treatment with vehicle (ethanol) or 75 µM sphingosine. Scale bar, 5 µm. (B) COS-7 cells were quantified for plasma membrane localization (see Materials and Methods) for the respective constructs following treatment with vehicle or 75 µM sphingosine. Three independent experiments were performed, and the error bars represent standard errors of the mean. *, $P < 0.0001$. (C) SDS-PAGE of supernatant (SN) and pellet (P) fractions collected from MLV sedimentation assays on lipid compositions shown above the gel. In all liposomes, 30 mol% POPE was used to maintain consistency, and the POPC levels were scaled accordingly when POPS or sphingosine was incorporated. (D) Quantification of MLV sedimentation assay results. The data represent the averages of three sedimentation assays, with the error bars representing the standard errors of the mean. *, $P < 0.05$.

head group, such as PS or PIP$_2$, for cellular localization (27, 60). We delivered sphingosine to the cells expressing EGFP-MARV VP40 in an attempt to neutralize the plasma membrane anionic charge. The delivery of sphingosine neutralized the plasma membrane negative charge successfully, as shown by the significant plasma membrane dissociation of the membrane charge sensor KR-ϕ, as previously reported (27) (Fig. 3). Similarly, EGFP-mVP40 exhibited a marked decrease in plasma membrane association in the presence of sphingosine, with redistribution to internal membranes. Redistribution of mVP40 from the plasma membrane to cytoplasmic membranes was not unexpected, because mVP40 is trafficked to the plasma membrane using an extensive network of internal membranes (14), and upon dissociation from the plasma membrane, it appears to reassociate with these internal membranes. This suggested that mVP40 association with the host cell plasma membrane is dependent on anionic charge sensing (Fig. 3).

We also monitored the effect of sphingosine on mVP40 interactions with membranes *in vitro*, using the MLV sedimentation assays. In these experiments, we measured the change in binding following incorporation of the positively charged sphingosine into MLVs that contained 30% POPS versus the effect of incorporating electrically neutral lipid molecules, such as diacylglycerol (DAG). The MLV assay results supported our cell-based assay data, as the incorporation of sphingosine into the MLVs led to marked reduction in the fraction of mVP40 that was associated with the MLVs (Fig. 3C and D). Incorporation of electrically neutral DAG did not decrease mVP40 association with MLVs that contained 30% POPS.

Increasing salt concentrations reduce electrostatic interactions between mVP40 and anionic membranes. The cellular and *in vitro* data examined above suggested mVP40 is an anionic charge sensor and is dependent on the anionic charge of the membrane to mediate its electrostatic interactions. To examine the effects of the salt concentration, which can influence electrostatic interactions, we monitored mVP40 binding to MLVs containing 30 mol% POPS in buffer containing increasing concentrations of KCl, from 150 mM to 1 M. As the KCl concentration was increased from a physiological level of ~150 mM to just 300 mM, binding of mVP40 diminished by approximately 2.5-fold (Fig. 4). The ability of a moderately high salt level to inhibit mVP40 membrane association strongly suggests that MARV VP40 interaction with lipid membranes is heavily dependent on electrostatic interactions.

Plasma membrane localization of mVP40 is partially dependent on PI(4,5)P$_2$. The plasma membrane inner leaflet contains a constitutive pool of PI(4,5)P$_2$ (29), as well as PI(4)P (28) and PIP$_3$ (61). In order to assess the importance of PI(4,5)P$_2$, which is the most abundant of the three PIPs in the plasma membrane inner leaflet and has also been implicated in other viral matrix protein interactions (40, 43, 44, 62), we monitored mVP40 localization in cells expressing a polyphosphoinositide 5-phosphatase IV (5-PtaseIV) and a catalytically inactive construct. The 5-PtaseIV selectively depletes plasma membrane PI(4,5)P$_2$ by hydrolyzing the phosphate group in the 5′ position of the inositol moiety, producing PI(4)P (44, 47, 63). It has been reported that there is an ~15-fold reduction in intracellular PI(4,5)P$_2$ levels in 293 cells that overexpress 5-PtaseIV (47). If a protein specifically binds to a PI(4,5)P$_2$ head group, depletion of the PI(4,5)P$_2$ pool leads to
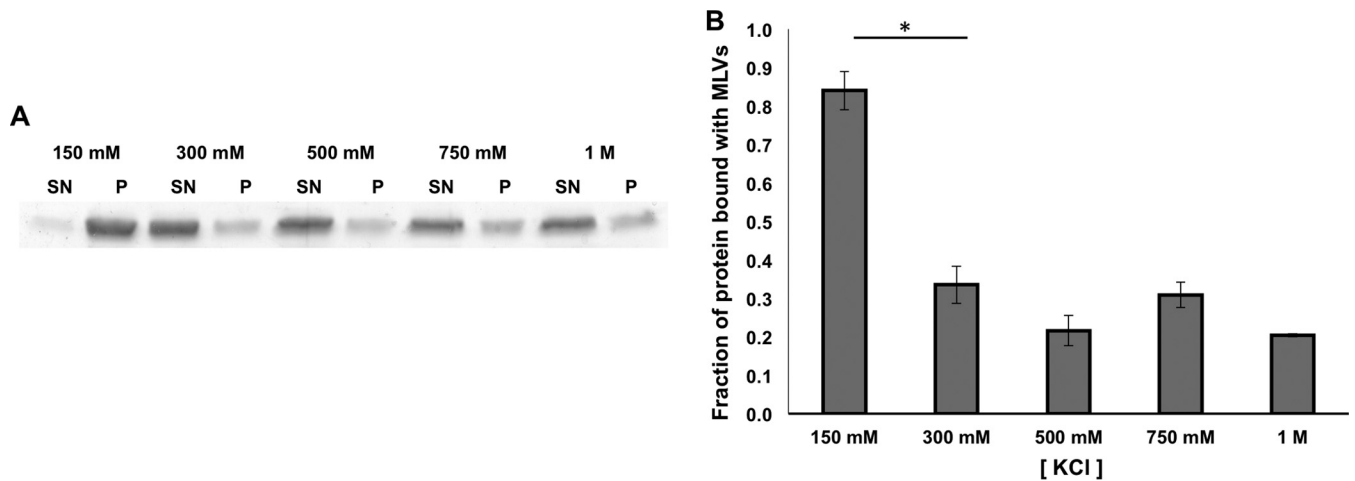
FIG 4 Increasing salt concentrations (KCl) diminished MARV VP40 association with anionic membranes. (A) SDS-PAGE of supernatant (SN) and pellet (P) fractions collected from MLV sedimentation assays that were performed in buffers that contained different KCl concentrations, as noted above the gel. All the liposomes consisted of POPC-POPE-POPS (40:30:30). (B) Quantification of MLV sedimentation assay results. The bars represent fractions of MARV VP40 associated with MLVs under different concentrations of KCl. The data represent the averages of three sedimentation assays, with the error bars representing the standard errors of the mean. *, $P < 0.05$.

dissociation of that protein from the plasma membrane, as is the case for the PLCδ-PH domain. The PH domain of this protein construct is specific for PI(4,5)P$_2$, and depletion of the PI(4,5)P$_2$ pool caused nearly complete dissociation from the plasma membrane (Fig. 5). For mVP40, depletion of the PI(4,5)P$_2$ pool led to only a small but statistically significant reduction in the plasma membrane localization (Fig. 5). A small degree of dissociation of mVP40 from the plasma membrane compared to PLCδ-PH reflects the loss of some anionic charges from the membrane due to depletion of the PI(4,5)P$_2$ pool (Fig. 5). A similar pattern of re-
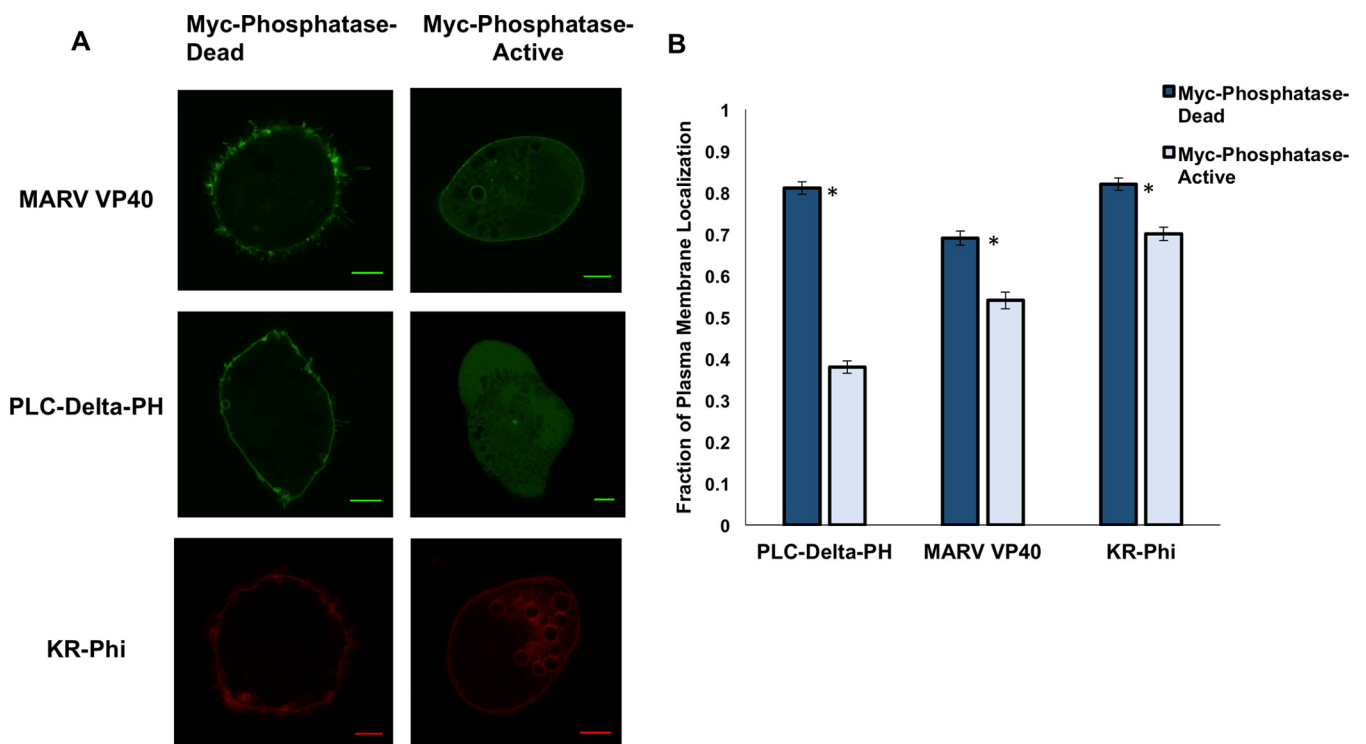

FIG 5 mVP40 plasma membrane localization in the presence of active or catalytically inactive 5-PtaseIV. (A) COS-7 cells expressing GFP fluorescent fusion constructs of MARV VP40, KR-ϕ-mRFP, or PLCδ-PH are shown 12 h posttransfection. The cells were cotransfected with active or a catalytically inactive (deletion mutant) 5-PtaseIV construct. Scale bars, 5 μm. (B) COS-7 cells were quantified for the average plasma membrane localization for the respective constructs in the presence of active 5-PtaseIV (light bars) or catalytically inactive 5-PtaseIV (dark bars). Three independent experiments were performed to determine the average localization and standard error of the mean. *, $P < 0.0001$.
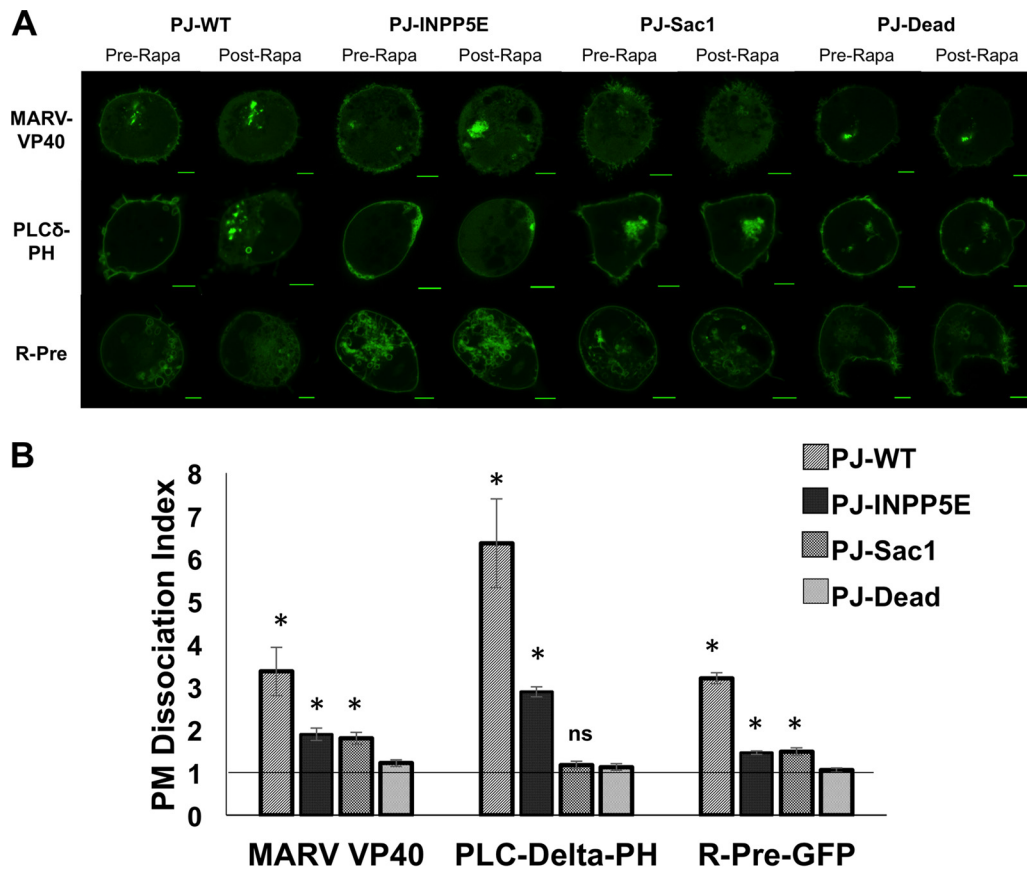
FIG 6 Changes in MARV VP40 localization in response to the real-time recruitment of different lipid phosphatase constructs to the plasma membrane inner leaflet. (A) Cos-7 cells expressing fluorescent fusion constructs of MARV VP40, PLCδ-PH, or R-Pre are shown 14 h posttransfection. The cells were cotransfected with a PJ-WT, PJ-INPP5E, PJ-SacI, or PJ-Dead construct, as well as a Lyn11 plasma membrane anchor. Pre-Rapa, images taken before the addition of rapamycin; Post-Rapa, images taken 7 min after addition of rapamycin. Scale bar, 5 μm. (B) Four independent real-time imaging experiments were performed for each construct to determine the standard error of the mean for each dissociation index ($n = 4$; confidence interval [CI] = 98%; ns, not significant; *, $P < 0.02$). The plasma membrane dissociation index was calculated as described in Materials and Methods using the following equation: dissociation index = (PM intensity/Cyto intensity)$_{before}$/(PM intensity/Cyto intensity)$_{after}$.

duction was observed for plasma membrane localization of the anionic charge sensor KR-φ (Fig. 5). Observing similar trends between mVP40 and the KR-φ protein further strengthened our conclusion that mVP40 behaves as an anionic charge sensor.

Next, we used a rapamycin-inducible PI(4,5)P$_2$ and PI(4)P depletion system generated by Hammond et al. to further confirm our observations on mVP40. The rapamycin-based PIP depletion can be used in real time to observe the effect of depleting PI(4,5)P$_2$, PI(4)P, or both at the plasma membrane inner leaflet on target proteins. The PJ-WT construct contains 5-phosphatase (INPP5E) and 4-phosphatase (Sac1) and causes rapid depletion of plasma membrane PI(4,5)P$_2$ and PI(4)P levels by hydrolyzing to PI upon recruitment of the PJ construct to the plasma membrane following addition of rapamycin. Proteins such as PLCδ-PH, which is specific to PI(4,5)P$_2$, show a sharp decrease in plasma membrane localization due to lack of substrate for its interaction, as shown in Fig. 6. R-Pre, another known anionic charge sensor (64), was used with the rapamycin-based PIP depletion system to compare charge-dependent behavior to that of mVP40. With mVP40, the effect of PJ-WT recruitment to the plasma membrane was about 2-fold lower in its dissociation index than that observed for PLCδ-PH (Fig. 6). This again suggests that mVP40 is depen-

dent on the anionic charge at the plasma membrane due to the enrichment of PI(4,5)P$_2$ and PI(4)P, which are hydrolyzed under the conditions of PJ-WT recruitment, but not to the level of PLCδ-PH displacement, as the PS and PI retained in the plasma membrane likely have sufficient anionic charge to mediate some of the mVP40 membrane association. mVP40 dissociation under these conditions was increased relative to the 5-PtaseIV depletion system, as under the rapamycin PJ-WT condition, both PI(4,5)P$_2$ and PI(4)P levels were drastically reduced (Fig. 5 and 6). With the PJ-WT depletion system, mVP40 and R-Pre displayed similar degrees of dissociation from the plasma membrane following addition of rapamycin (the plasma membrane dissociation indexes for mVP40 and R-Pre were 3.56 and 3.2, respectively) (Fig. 6).

The PJ-INPP5E construct, which contains the active 5-phosphatase and inactive 4-phosphatase, hydrolyzes PI(4,5)P$_2$ to PI(4)P and was used to assess PLCδ-PH, mVP40, and R-Pre plasma membrane dissociation following rapamycin addition (Fig. 6). The effect of depletion of PI(4,5)P$_2$ to PI(4)P also greatly induced dissociation of PLCδ-PH from the plasma membrane (Fig. 6). mVP40 and R-Pre also dissociated from the plasma membrane when PI(4,5)P$_2$ was selectively depleted to PI(4)P by PJ-INPP5E but not to the same extent as when both PI(4,5)P$_2$ and
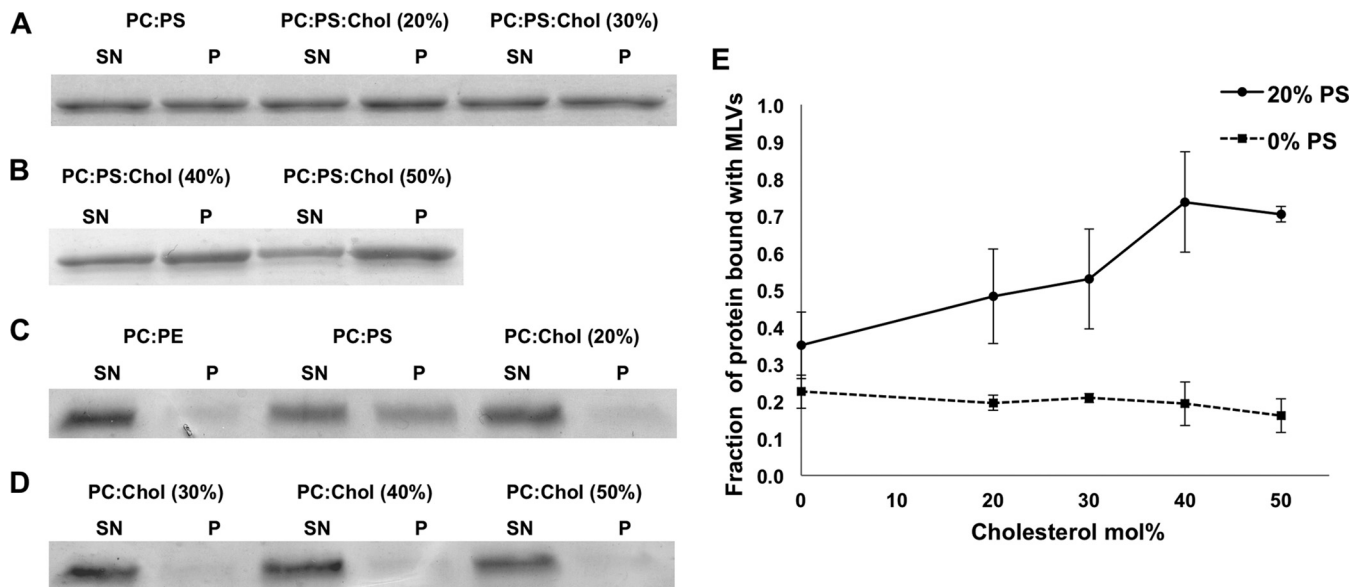
FIG 7 Influence of cholesterol on MARV VP40 association with POPS-containing membranes. (A to D) SDS-PAGE of supernatant (SN) and pellet (P) fractions collected from MLV sedimentation assays on lipid compositions shown above the gels. In all liposomes, 30 mol% POPE was used, and when mentioned, 20 mol% POPS was used to maintain consistency. (A and B) MARV VP40 shows enhanced association with MLVs that contain 20% POPS in response to the cholesterol (Chol) gradient. (C and D) Cholesterol in the absence of POPS does not promote significant association of mVP40 with MLVs. (E) Quantification of MLV sedimentation assay results with Image J. The data represent the averages of three sedimentation assays, with the error bars representing the standard errors of the mean. CI = 95%.

PI(4)P were depleted with PJ-WT. The fold decreases in the dissociation index were similar for mVP40 and PLCδ-PH when PJ-INPP5E data were compared to those of PJ-WT (Fig. 6). Under conditions of PJ-INPP5E activity, PI(4)P levels are presumably still intact to allow for more PI(4,5)P$_2$ formation from PI(4)P by the PI(4)P 5-kinase. Additionally, the total plasma membrane anionic content is lowered only by removal of the 5-phosphate supporting the more significant plasma membrane retention of mVP40 and R-Pre compared to the PJ-WT experiments. The lower dissociation index for R-Pre than for mVP40 for PJ-INPP5E experiments may be due to the lipidation present on the R-Pre protein that can interact with acyl chains of phospholipids and provide additional stability to R-Pre at the plasma membrane.

Next, we employed a construct with an active 4-phosphatase but an inactive 5-phosphatase, PJ-Sac1, which has been shown to selectively deplete plasma membrane PI(4)P following rapamycin addition. Under these conditions, the PLCδ-PH plasma membrane dissociation was not affected, as PI(4)P is hydrolyzed to PI (Fig. 6). However, PJ-Sac1 activity did induce dissociation of mVP40 from the plasma membrane to a similar degree as the PJ-INPP5E construct. This is also consistent with the principle that PJ-Sac1 and PJ-INPP5E reduce the plasma membrane anionic charge to similar degrees (i.e., removal of one phosphate each). R-Pre also had a statistically significant increase in dissociation from the plasma membrane when PJ-Sac1 was active and to a level similar to that of the PJ-INPP5E-induced dissociation. Once again, the lower dissociation index of R-Pre can be attributed to its lipid anchor. A catalytically inactive 5-phosphatase and 4-phosphatase construct, PJ-DEAD, was also used as a negative control to compare and normalize the dissociation index for each construct (Fig. 6).

The cell-based data collected here are consistent with the *in vitro* data, suggesting broad binding to anionic lipids by mVP40, which includes PS, PI(4,5)P$_2$, and possibly PI(4)P and PA enriched on the plasma membrane inner leaflet. Taken together, the *in vitro* and cellular experiments demonstrated that mVP40 is promiscuous in its selectivity for anionic phospholipids and is a membrane anionic charge sensor.

Cholesterol enhances association of MARV VP40 with membranes that contain PS. It has been reported that HIV-1 GAG, which contains the matrix lipid binding domain, shows enhanced association with membranes that contain cholesterol (41). We investigated if cholesterol was able to enhance binding of mVP40 using the MLV sedimentation assay. First, we increased the cholesterol content of MLVs that contained 20% POPS from 0% to 50%, which is below the solubility limit of cholesterol in POPC- and POPE-containing vesicles (41, 65). As the cholesterol content increased, mVP40 association with the membranes also increased, reaching a maximum binding level at ~40% cholesterol content in the MLVs (Fig. 7 A, B, and E). Next, we removed POPS from the MLVs to investigate if mVP40 responds to the cholesterol gradient in the absence of anionic lipids. As shown in Fig. 7, mVP40 did not significantly associate with MLVs containing increasing concentrations of cholesterol but devoid of POPS (Fig. 7C, D, and E). This again suggests the necessity for anionic charge at the membrane to recruit mVP40 via electrostatic interactions. The increased association of mVP40 in the presence of cholesterol may be due to the phenomenon known as the "cholesterol condensation effect" (41, 66). Increasing concentrations of cholesterol result in tighter packing of acyl chains, causing the phospholipid head groups to pack closely, as well. As a result of the increase in the packing density of phospholipid head groups, clustering of anionic POPS in the membranes may appear to be greater than in the absence of cholesterol. This apparent increase in regions of

anionic charge density is likely sufficient to recruit mVP40 and hence cause an increase in membrane association at lower levels of POPS.

DISCUSSION

Despite the discovery of MARV in 1967 ([2], [67], [68]), little information is available on its matrix protein interactions with host proteins or lipids. To our knowledge, we present the first analysis of mVP40 interactions with lipids. Here, we found that mVP40 associates with membranes using nonspecific electrostatic interactions and that the binding saturates at a negative charge density of ~40 to 45%, regardless of the lipid head group employed. This mechanism was responsible for the plasma membrane localization of mVP40, as neutralization of the plasma membrane charge led to redistribution of mVP40 to internal membranes.

The first clue to mVP40 promiscuity in its interaction with anionic phospholipids came from MLV assay data that examined association with membranes that contain 20% PS and 5% PIPs. In this data set, we observed that mVP40 associated similarly with vesicles containing three different types of monophosphates [PI(3)P, PI(4)P, and PI(5)P]. mVP40 behaved similarly when the bisphosphate derivatives of PIPs [PI(3,4)P$_2$, PI(4,5)P$_2$, and PI(3,5)P$_2$] were employed. Here, mVP40 associated similarly, regardless of the position of the phosphate groups. Similarly, when PIP$_3$ was included in the vesicles, mVP40 demonstrated a further increase in binding compared to the bisphosphates. Further, when 20% PS and 5% PIPs were included in the same vesicles, the combined effect of PS and PIPs was additive, further suggesting dependency on the membrane anionic charge density for mVP40 binding.

The notion of mVP40 functioning as an anionic charge sensor was further validated with overlap of the mVP40 binding curves with different anionic phospholipids [PS, PA, PI(4)P, and PI(4,5)P$_2$] following their charge correction. *In vitro* assay data were supported with live-cell assays using sphingosine, where neutralization of the plasma membrane negative charge caused a dramatic reduction in localization of mVP40. Depletion of the PI(4,5)P$_2$ pool in the plasma membrane by 5-PtaseIV reduced the plasma membrane localization of mVP40, but by ~18% compared to an ~54% reduction for PLCδ-PH. Reduction of the plasma membrane localization for the known anionic charge sensor KR-ϕ due to 5-PtaseIV was ~16%, which is very similar to the dissociation shown by mVP40. Moreover, the background GFP signal at the plasma membrane for PLCδ-PH when PI(4,5)P$_2$ is depleted was comparable to that of GFP alone. This suggested that mVP40 lacks stereospecific interaction with PI(4,5)P$_2$ in the plasma membrane and behaves more like KR-ϕ, which associates with the plasma membrane in an electrostatic manner devoid of any stereospecific association. Rather, the modest but statistically significant reduction in mVP40 plasma membrane localization was due to the loss of the anionic charge contribution by the phosphate group on the 5′ position of the inositol moiety on PI(4,5)P$_2$ (Fig. 5 and 6). This loss of a single phosphate group results in loss of additional anionic charge. However, the pool of PI(4,5)P$_2$ is likely to be 3 to 5 mol% in the plasma membrane, and although the contribution of anionic charges from PI(4,5)P$_2$ to the plasma membrane is significant, PS may be found at 15 to 20 mol% of the plasma membrane inner leaflet and represents ~30% of the anionic charge. This 30% anionic charge is similar to the level of charge that would promote ~75 to 85% mVP40 binding *in vitro*.

From the recent crystal structure of the mVP40 dimer ([26]), the CTD harbors the purported lipid binding surface or the basic patch of the protein. The mVP40 dimer is flatter and contains a basic patch larger than that of eVP40. The positively charged side chains of Arg and Lys residues comprising the basic patch seem to project outward and away from the flat surfaces of the CTD domains of the mVP40 dimer. These structural features of mVP40 are consistent with the membrane interaction data we found in this study. The cationic amino acid side chains that project away from the CTD surface provide ideal sites to form salt bridges with the anionic phospholipid head groups and mediate membrane interactions. Our data support the idea that mVP40 interactions with the membrane rely heavily on electrostatic effects, which is further supported in the structural analysis, where single mutation of Lys210 to Glu abrogated VLP formation ([26]). Moreover, we have demonstrated that the K210E construct binding to vesicles containing PS was ~30% reduced while binding of double and triple mutations of the mVP40 cationic patch was nearly fully abrogated ([26]). Binding of mVP40 was also restored by a K210R construct, further suggesting that nonspecific electrostatic interactions play an important role in membrane association, as Arg seemed to substitute for Lys *in vitro* and in cells ([26]). Additionally, abrogation of the mVP40 dimer interface (T105R mutation) significantly reduced binding to vesicles containing PS, suggesting the extensive cationic patch provided by two CTDs when the VP40 dimer is intact ([26]) is necessary for anionic charge sensing. The lipid binding studies with T105R further suggested that the nonspecific electrostatic association observed for mVP40 in the study was not simply due to lack of proper folding of the CTD domain and subsequent nonspecific binding. These data again underscore the need for multiple electrostatic interactions between lipid head groups in the plasma membrane and the cationic patch in the mVP40 dimer ([26]). While targeting nonspecific electrostatic interactions would be difficult therapeutically ([69]), staurosporines ([70]–[72]), derivatives of which are in clinical trial ([73], [74]), have been shown to block endosomal sorting and recycling of PS. This decreased the plasma membrane PS pool and altered the localization of proteins dependent on electrostatic interactions with the plasma membrane ([71], [72]).

While some structure-function data on eVP40 are available, almost nothing is known about mVP40 membrane interactions. Comparison of the eVP40 and mVP40 sequences revealed amino acid sequence identity of 34%, with even less identity in the CTD membrane binding region. These sequence dissimilarities seem to contribute to the different lipid binding properties of eVP40 and mVP40. Previous studies have demonstrated that eVP40 can associate with vesicles containing PS ([20], [22]–[24], [38]). While these previous studies have not discriminated between specific and nonspecific electrostatic interactions with PS, more detailed experiments with PS interactions in cell culture have demonstrated that PS plays an important and specific role in interacting with eVP40 ([59], [60]). Additionally, treatment of human and mammalian cell lines expressing eVP40 with sphingosine did not have a significant effect on eVP40 plasma membrane localization ([59], [60]). These studies have strongly suggested that eVP40 membrane association is not a simple case of anionic charge sensing. This suggests that though mVP40 and eVP40 both rely heavily on electrostatic interactions for membrane association, there is a fundamental difference between the two proteins' mechanism of assembly at the plasma membrane. Many peripheral proteins rely on

more than electrostatic interactions for membrane targeting (75), and while it is quite possible the mVP40 dimer electrostatic interactions with the plasma membrane are sufficient to drive NTD displacement and mVP40 oligomerization, further biophysical analysis is warranted to understand the mechanisms of lipid-protein and protein-protein interactions that regulate the mVP40 matrix assembly.

ACKNOWLEDGMENTS

FUNDING INFORMATION

REFERENCES

1. **Rougeron V, Feldmann H, Grard G, Becker S, Leroy EM.** 2015. Ebola and Marburg haemorrhagic fever. J Clin Virol **64**:111–119. http://dx.doi.org/10.1016/j.jcv.2015.01.014.
2. **Peters D, Muller G, Slenccka W.** 1971. Morphology, development, and classification of the Marburg virus. Springer, Berlin, Germany.
3. **Geisbert TW, Jahrling PB.** 1995. Differentiation of filoviruses by electron microscopy. Virus Res **39**:129–150. http://dx.doi.org/10.1016/0168-1702(95)00080-1.
4. **Feldmann H, Muhlberger E, Randolf A, Will C, Kiley MP, Sanchez A, Klenk HD.** 1992. Marburg virus, a filovirus: messenger-RNAs, gene order, and regulatory elements of the replication cycle. Virus Res **24**:1–19. http://dx.doi.org/10.1016/0168-1702(92)90027-7.
5. **Jasenosky LD, Neumann G, Lukashevich I, Kawaoka Y.** 2001. Ebola virus VP40-induced particle formation and association with the lipid bilayer. J Virol **75**:5205–5214. http://dx.doi.org/10.1128/JVI.75.11.5205-5214.2001.
6. **Licata JM, Johnson RF, Han ZY, Harty RN.** 2004. Contribution of Ebola virus glycoprotein, nucleoprotein, and VP24 to budding of VP40 virus-like particles. J Virol **78**:7344–7351. http://dx.doi.org/10.1128/JVI.78.14.7344-7351.2004.
7. **Noda T, Sagara H, Suzuki E, Takada A, Kida H, Kawaoka Y.** 2002. Ebola virus VP40 drives the formation of virus-like filamentous particles along with GP. J Virol **76**:4855–4865. http://dx.doi.org/10.1128/JVI.76.10.4855-4865.2002.
8. **Timmins J, Scianimanico S, Schoehn G, Weissenhorn W.** 2001. Vesicular release of Ebola virus matrix protein VP40. Virology **283**:1–6. http://dx.doi.org/10.1006/viro.2001.0860.
9. **Muhlberger E, Lotfering B, Klenk HD, Becker S.** 1998. Three of four nucleocapsid proteins of Marburg virus, NP, VP35, and L, are sufficient to mediate replication and transcription of Marburg virus-specific monocistronic minigenomes. J Virol **72**:8756–8764.
10. **Valmas C, Basler CF.** 2011. Marburg virus VP40 antagonizes interferon signaling in a species-specific manner. J Virol **85**:4309–4317. http://dx.doi.org/10.1128/JVI.02575-10.
11. **Hoenen T, Jung S, Herwig A, Groseth A, Becker S.** 2010. Both matrix proteins of Ebola virus contribute to the regulation of viral genome replication and transcription. Virology **403**:56–66. http://dx.doi.org/10.1016/j.virol.2010.04.002.
12. **Wenigenrath J, Kolesnikova L, Hoenen T, Mittler E, Becker S.** 2010. Establishment and application of an infectious virus-like particle system for Marburg virus. J Gen Virol **91**:1325–1334. http://dx.doi.org/10.1099/vir.0.018226-0.
13. **Kolesnikova L, Ryabchikova E, Shestopalov A, Becker S.** 2007. Basolateral budding of Marburg virus: VP40 retargets viral glycoprotein GP to the basolateral surface. J Infect Dis **196**:S232–S236. http://dx.doi.org/10.1086/520584.
14. **Kolesnikova L, Bugany H, Klenk HD, Becker S.** 2002. VP40, the matrix protein of Marburg virus is associated with membranes of the late endosomal compartment. J Virol **76**:1825–1838. http://dx.doi.org/10.1128/JVI.76.4.1825-1838.2002.
15. **Yamayoshi S, Noda T, Ebihara H, Goto H, Morikawa Y, Lukashevich IS, Neurnann G, Feldmann H, Kawaoka Y.** 2008. Ebola virus matrix protein VP40 uses the COPII transport system for its intracellular transport. Cell Host Microbe **3**:168–177. http://dx.doi.org/10.1016/j.chom.2008.02.001.
16. **Dessen A, Volchkov V, Dolnik O, Klenk HD, Weissenhorn W.** 2000. Crystal structure of the matrix protein VP40 from Ebola virus. EMBO J **19**:4228–4236. http://dx.doi.org/10.1093/emboj/19.16.4228.
17. **Gomis-Rüth FX, Dessen A, Timmins J, Bracher A, Kolesnikowa L, Becker S, Klenk HD, Weissenhorn W.** 2003. The matrix protein VP40 from Ebola virus octamerizes into pore-like structures with specific RNA binding properties. Structure **11**:423–433. http://dx.doi.org/10.1016/S0969-2126(03)00050-9.
18. **Hoenen T, Volchkov V, Kolesnikova L, Mittler E, Timmins J, Ottmann M, Reynard O, Becker S, Weissenhorn W.** 2005. VP40 octamers are essential for Ebola virus replication. J Virol **79**:1898–1905. http://dx.doi.org/10.1128/JVI.79.3.1898-1905.2005.
19. **Timmins J, Schoehn G, Kohlhaas C, Klenk HD, Ruigrok RWH, Weissenhorn W.** 2003. Oligomerization and polymerization of the filovirus matrix protein VP40. Virology **312**:359–368. http://dx.doi.org/10.1016/S0042-6822(03)00260-5.
20. **Adu-Gyamfi E, Soni SP, Xue Y, Digman MA, Gratton E, Stahelin RV.** 2013. The Ebola virus matrix protein penetrates into the plasma membrane, a key step in viral protein 40 (VP40) oligomerization and viral egress. J Biol Chem **288**:5779–5789. http://dx.doi.org/10.1074/jbc.M112.443960.
21. **Bornholdt ZA, Noda T, Abelson DM, Halfmann P, Wood MR, Kawaoka Y, Saphire EO.** 2013. Structural rearrangement of Ebola virus VP40 begets multiple functions in the virus life cycle. Cell **154**:763–774. http://dx.doi.org/10.1016/j.cell.2013.07.015.
22. **Ruigrok RWH, Schoehn G, Dessen A, Forest E, Volchkov V, Dolnik O, Klenk HD, Weissenhorn W.** 2000. Structural characterization and membrane binding properties of the matrix protein VP40 of Ebola virus. J Mol Biol **300**:103–112. http://dx.doi.org/10.1006/jmbi.2000.3822.
23. **Scianimanico S, Schoehn G, Timmins J, Ruigrok RHW, Klenk HD, Weissenhorn W.** 2000. Membrane association induces a conformational change in the Ebola virus matrix protein. EMBO J **19**:6732–6741. http://dx.doi.org/10.1093/emboj/19.24.6732.
24. **Soni SP, Adu-Gyamfi E, Yong SS, Jee CS, Stahelin RV.** 2013. The Ebola virus matrix protein deeply penetrates the plasma membrane: an important step in viral egress. Biophys J **104**:1940–1949. http://dx.doi.org/10.1016/j.bpj.2013.03.021.
25. **Stahelin RV.** 2014. Membrane binding and bending in Ebola VP40 assembly and egress. Front Microbiol **5**:300. http://dx.doi.org/10.3389/fmicb.2014.00300.
26. **Oda SI, Noda T, Wijesinghe KJ, Halfmann P, Bornholdt ZA, Abelson DM, Armbrust T, Stahelin RV, Kawaoka Y, Saphire EO.** 9 December 2015. Crystal structure of Marburg virus VP40: matrix assembly and immunosuppression. J Virol. http://dx.doi.org/10.1128/JVI.01597-15.
27. **Yeung T, Gilbert GE, Shi J, Silvius J, Kapus A, Grinstein S.** 2008. Membrane phosphatidylserine regulates surface charge and protein localization. Science **319**:210–213. http://dx.doi.org/10.1126/science.1152066.
28. **Hammond GRV, Fischer MJ, Anderson KE, Holdich J, Koteci A, Balla T, Irvine RF.** 2012. PI4P and PI(4,5)P-2 are essential but independent lipid determinants of membrane identity. Science **337**:727–730. http://dx.doi.org/10.1126/science.1222483.
29. **Balla T.** 2013. Phosphoinositides: tiny lipids with giant impact on cell regulation. Physiol Rev **93**:1019–1137. http://dx.doi.org/10.1152/physrev.00028.2012.
30. **McLaughlin S, Murray D.** 2005. Plasma membrane phosphoinositide organization by protein electrostatics. Nature **438**:605–611. http://dx.doi.org/10.1038/nature04398.
31. **McLaughlin S, Wang JY, Gambhir A, Murray D.** 2002. PIP2 and proteins: interactions, organization, and information flow. Annu Rev Biophys Biomol Struct **31**:151–175. http://dx.doi.org/10.1146/annurev.biophys.31.082901.134259.
32. **Vance JE, Steenbergen R.** 2005. Metabolism and functions of phosphatidyl-

serine. Prog Lipid Res **44:**207–234. http://dx.doi.org/10.1016/j.plipres.2005 .05.001.

33. **Cho W, Stahelin RV.** 2006. Membrane binding and subcellular targeting of C2 domains. Biochim Biophys Acta **1761:**838–849. http://dx.doi.org /10.1016/j.bbalip.2006.06.014.

34. **Wang JY, Gambhir A, Hangyas-Mihalyne G, Murray D, Golebiewska U, McLaughlin S.** 2002. Lateral sequestration of phosphatidylinositol 4,5-bisphosphate by the basic effector domain of myristoylated alanine-rich C kinase substrate is due to nonspecific electrostatic interactions. J Biol Chem **277:**34401–34412. http://dx.doi.org/10.1074/jbc.M203954200.

35. **Hammond GRV, Balla T.** 2015. Polyphosphoinositide binding domains: key to inositol lipid biology. Biochim Biophys Acta **1851:**746–758. http://dx.doi.org/10.1016/j.bbalip.2015.02.013.

36. **Cho WH, Stahelin RV.** 2005. Membrane-protein interactions in cell signaling and membrane trafficking. Annu Rev Biophys Biomol Struct **34:**119–151. http://dx.doi.org/10.1146/annurev.biophys.33.110502.133337.

37. **Moravcevic K, Oxley CL, Lemmon MA.** 2012. Conditional peripheral membrane proteins: facing up to limited specificity. Structure **20:**15–27. http://dx.doi.org/10.1016/j.str.2011.11.012.

38. **Soni SP, Stahelin RV.** 2014. The Ebola virus matrix protein VP40 selectively induces vesiculation from phosphatidylserine-enriched membranes. J Biol Chem **289:**33590–33597. http://dx.doi.org/10.1074 /jbc.M114.586396.

39. **Chukkapalli V, Inlora J, Todd GC, Ono A.** 2013. Evidence in support of RNA-mediated inhibition of phosphatidylserine-dependent HIV-1 Gag membrane binding in cells. J Virol **87:**7155–7159. http://dx.doi.org/10 .1128/JVI.00075-13.

40. **Chukkapalli V, Oh SJ, Ono A.** 2010. Opposing mechanisms involving RNA and lipids regulate HIV-1 Gag membrane binding through the highly basic region of the matrix domain. Proc Natl Acad Sci U S A **107:** 1600–1605. http://dx.doi.org/10.1073/pnas.0908661107.

41. **Dick RA, Goh SL, Feigenson GW, Vogt VM.** 2012. HIV-1 Gag protein can sense the cholesterol and acyl chain environment in model membranes. Proc Natl Acad Sci U S A **109:**18761–18766. http://dx.doi.org/10 .1073/pnas.1209408109.

42. **Dick RA, Kamynina E, Vogt VM.** 2013. Effect of multimerization on membrane association of Rous sarcoma virus and HIV-1 matrix domain proteins. J Virol **87:**13598–13608. http://dx.doi.org/10.1128/JVI .01659-13.

43. **Ono A.** 2010. HIV-1 assembly at the plasma membrane. Vaccine **28**(Suppl 2):B55–B59. http://dx.doi.org/10.1016/j.vaccine.2009.10.021.

44. **Ono A, Ablan SD, Lockett SJ, Nagashima K, Freed EO.** 2004. Phosphatidylinositol(4,5)bisphosphate regulates HIV-1 gag targeting to the plasma membrane. Proc Natl Acad Sci U S A **101:**14889–14894. http://dx.doi.org/10.1073/pnas.0405596101.

45. **Vlach J, Saad JS.** 2013. Trio engagement via plasma membrane phospholipids and the myristoyl moiety governs HIV-1 matrix binding to bilayers. Proc Natl Acad Sci U S A **110:**3525–3530. http://dx.doi.org/10.1073/pnas .1216655110.

46. **Zakowski JJ, Petri WA, Wagner RR.** 1981. Role of matrix protein in assembling the membrane of vesicular stomatitis virus: reconstitution of matrix protein with negatively charged phospholipid vesicles. Biochemistry **20:**3902–3907. http://dx.doi.org/10.1021/bi00516a037.

47. **Kisseleva MV, Cao L, Majerus PW.** 2002. Phosphoinositide-specific inositol polyphosphate 5-phosphatase IV inhibits Akt/protein kinase B phosphorylation and leads to apoptotic cell death. J Biol Chem **277:**6266–6272. http://dx.doi.org/10.1074/jbc.M105969200.

48. **Bangham AD, Horne RW.** 1964. Negative staining of phospholipids and their structural modification by surface active agents as observed in electron microscope. J Mol Biol **8:**660–668. http://dx.doi.org/10.1016/S0022 -2836(64)80115-7.

49. **Papahadjopoulos D, Watkins JC.** 1967. Phospholipid model membranes. II. Permeability properties of hydrated liquid crystals. Biochim Biophys Acta **135:**639–652.

50. **Patil YP, Jadhav S.** 2014. Novel methods for liposome preparation. Chem Phys Lipids **177:**8–18. http://dx.doi.org/10.1016/j.chemphyslip.2013.10 .011.

51. **Saarikangas J, Zhao HX, Pykalainen A, Laurinmaki P, Mattila PK, Kinnunen PKJ, Butcher SJ, Lappalainen P.** 2009. Molecular mechanisms of membrane deformation by I-BAR domain proteins. Curr Biol **19:**95–107. http://dx.doi.org/10.1016/j.cub.2008.12.029.

52. **Mattila PK, Pykalainen A, Saarikangas J, Paavilainen VO, Vihinen H, Jokitalo E, Lappalainen P.** 2007. Missing-in-metastasis and IRSp53

deform PI(4,5)P-2-rich membranes by an inverse BAR domain-like mechanism. J Cell Biol **176:**953–964. http://dx.doi.org/10.1083/jcb .200609176.

53. **Kooijman EE, King KE, Gangoda M, Gericke A.** 2009. Ionization properties of phosphatidylinositol polyphosphates in mixed model membranes. Biochemistry **48:**9360–9371. http://dx.doi.org/10.1021/bi9008616.

54. **Kooijman EE, Carter KM, van Laar EG, Chupin V, Burger KNJ, de Kruijff B.** 2005. What makes the bioactive lipids phosphatidic acid and lysophosphatidic acid so special? Biochemistry **44:**17007–17015. http://dx .doi.org/10.1021/bi0518794.

55. **Parasassi T, De Stasio G, Ravagnan G, Rusch RM, Gratton E.** 1991. Quantitation of lipid phases in phospholipid-vesicles by the generalized polarization of Laurdan fluorescence. Biophys J **60:**179–189. http://dx.doi .org/10.1016/S0006-3495(91)82041-0.

56. **Parasassi T, Distefano M, Loiero M, Ravagnan G, Gratton E.** 1994. Cholesterol modifies water concentration and dynamics in phospholipid bilayers: a fluorescence study using Laurdan probe. Biophys J **66:**763–768. http://dx.doi.org/10.1016/S0006-3495(94)80852-5.

57. **Harris FM, Best KB, Bell JD.** 2002. Use of laurdan fluorescence intensity and polarization to distinguish between changes in membrane fluidity and phospholipid order. Biochim Biophys Acta **1565:**123–128. http://dx.doi .org/10.1016/S0005-2736(02)00514-X.

58. **Ramani K, Balasubramanian SV.** 2003. Fluorescence properties of Laurdan in cochleate phases. Biochim Biophys Acta **1618:**67–78. http://dx.doi .org/10.1016/j.bbamem.2003.10.009.

59. **Adu-Gyamfi E, Johnson KA, Fraser ME, Scott JL, Soni SP, Jones KR, Digman MA, Gratton E, Tessier CR, Stahelin RV.** 2015. Host cell plasma membrane phosphatidylserine regulates the assembly and budding of Ebola virus. J Virol **89:**9440–9453. http://dx.doi.org/10.1128 /JVI.01087-15.

60. **Johnson KA, Taghon GJ, Scott JL, Stahelin RV.** 2016. The Ebola virus matrix protein, VP40, requires phosphatidylinositol 4,5-bisphosphate (PI(4,5)P2) for extensive oligomerization at the plasma membrane and viral egress. Sci Rep **6:**19125. http://dx.doi.org/10.1038/srep19125.

61. **Heo WD, Inoue T, Park WS, Kim ML, Park BO, Wandless TJ, Meyer T.** 2006. PI(3,4,5)P-3 and PI(4,5)P-2 lipids target proteins with polybasic clusters to the plasma membrane. Science **314:**1458–1461. http://dx.doi .org/10.1126/science.1134389.

62. **Ono A.** 2009. HIV-1 assembly at the plasma membrane: Gag trafficking and localization. Future Virol **4:**241–257. http://dx.doi.org/10 .2217/fvl.09.4.

63. **Chukkapalli V, Hogue IB, Boyko V, Hu WS, Ono A.** 2008. Interaction between the human immunodeficiency virus type 1 Gag matrix domain and phosphatidylinositol-(4,5)-bisphosphate is essential for efficient Gag membrane binding. J Virol **82:**2405–2417. http://dx.doi.org/10.1128/JVI .01614-07.

64. **Yeung T, Terebiznik M, Yu LM, Silvius J, Abidi WM, Philips M, Levine T, Kapus A, Grinstein S.** 2006. Receptor activation alters inner surface potential during phagocytosis. Science **313:**347–351. http://dx.doi.org/10 .1126/science.1129551.

65. **Huang JY, Buboltz JT, Feigenson GW.** 1999. Maximum solubility of cholesterol in phosphatidylcholine and phosphatidylethanolamine bilayers. Biochim Biophys Acta **1417:**89–100. http://dx.doi.org/10.1016/S0005 -2736(98)00260-0.

66. **Huang JY, Feigenson GW.** 1999. A microscopic interaction model of maximum solubility of cholesterol in lipid bilayers. Biophys J **76:**2142–2157. http://dx.doi.org/10.1016/S0006-3495(99)77369-8.

67. **Murphy FA, Simpson DIH, Whitfield S, Zlotnik I, Carter GB.** 1971. Marburg virus infection in monkeys: ultrastructural studies. Lab Invest **24:**279–291.

68. **Smith CE.** 1971. Lessons from Marburg disease. Sci Basis Med Annu Rev **1971:**58–80.

69. **Stahelin RV.** 2014. Could the Ebola virus matrix protein VP40 be a drug target? Expert Opin Ther Targets **18:**115–120. http://dx.doi.org/10.1517 /14728222.2014.863877.

70. **Cho KJ, Park JH, Hancock JF.** 2013. Staurosporine: a new tool for studying phosphatidylserine trafficking. Commun Integr Biol **6:**e24746. http://dx.doi.org/10.4161/cib.24746.

71. **Cho KJ, Park JH, Piggott AM, Salim AA, Gorfe AA, Parton RG, Capon RJ, Lacey E, Hancock JF.** 2012. Staurosporines disrupt phosphatidylserine trafficking and mislocalize Ras proteins. J Biol Chem **287:**43573–43584. http://dx.doi.org/10.1074/jbc.M112.424457.

72. **Cho KJ, van der Hoeven D, Hancock JF.** 2013. Inhibitors of K-Ras plasma membrane localization. Enzymes **33:**249–265. http://dx.doi.org/10.1016/B978-0-12-416749-0.00011-7.

73. **Gojo I, Perl A, Luger S, Baer MR, Norsworthy KJ, Bauer KS, Tidwell M, Fleckinger S, Carroll M, Sausville EA.** 2013. Phase I study of UCN-01 and perifosine in patients with relapsed and refractory acute leukemias and high-risk myelodysplastic syndrome. Invest New Drugs **31:**1217–1227. http://dx.doi.org/10.1007/s10637-013-9937-8.

74. **Ma CX, Ellis MJ, Petroni GR, Guo Z, Cai SR, Ryan CE, Craig Lockhart A, Naughton MJ, Pluard TJ, Brenin CM, Picus J, Creekmore AN, Mwandoro T, Yarde ER, Reed J, Ebbert M, Bernard PS, Watson M, Doyle LA, Dancey J, Piwnica-Worms H, Fracasso PM.** 2013. A phase II study of UCN-01 in combination with irinotecan in patients with metastatic triple negative breast cancer. Breast Cancer Res Treat **137:**483–492. http://dx.doi.org/10.1007/s10549-012-2378-9.

75. **Whited AM, Johs A.** 2015. The interactions of peripheral membrane proteins with biological membranes. Chem Phys Lipids **192:**51–59. http://dx.doi.org/10.1016/j.chemphyslip.2015.07.015.